Raman and x-ray diffraction studies of nanometric $Sn_2P_2S_6$ crystals

2003 J. Phys.: Condens. Matter 15 6381

(http://iopscience.iop.org/0953-8984/15/37/006)

INSTITUTE OF PHYSICS PUBLISHING JOURNAL OF PHYSICS: CONDENSED MATTER

J. Phys.: Condens. Matter **15** (2003) 6381–6393 PII: S0953-8984(03)60541-2

Raman and x-ray diffraction studies of nanometric $Sn_2P_2S_6$ crystals

A V Gomonnai[1], Yu M Azhniuk[1], Yu M Vysochanskii[2], A A Kikineshi[2], M Kis-Varga[3], L Daroczy[4], I P Prits[2] and I M Voynarovych[2]

[1] Institute of Electron Physics, Ukrainian National Academy of Science, Universytetska Street 21, Uzhhorod 88017, Ukraine
[2] Uzhhorod National University, Pidhirna Street 46, Uzhhorod 88000, Ukraine
[3] Institute of Nuclear Research, Hungarian Academy of Science, PO Box 51, 4001 Debrecen, Hungary
[4] Department of Solid State Physics, University of Debrecen, PO Box 2, 4010 Debrecen, Hungary

E-mail: azhn@ukrpost.net and azh@iep.uzhgorod.ua

Received 25 February 2003
Published 8 September 2003
Online at stacks.iop.org/JPhysCM/15/6381

Abstract

Nanometric $Sn_2P_2S_6$ crystalline powders and ceramics are studied by x-ray diffraction and Raman spectroscopy. The average crystallite size is estimated from TEM and x-ray data. The observed features in the Raman spectra are discussed in view of confinement-related selection rules relaxation, surface phonon modes and possible partial substitution of sulfur by oxygen at the nanometric powder surface.

1. Introduction

The last decade of the previous century gave rise to a keen interest in the studies of semiconductor microcrystals whose specific properties, resulting from the spatial confinement of charge carriers, have determined a wide variety of promising application possibilities. X-ray diffraction (XRD) and Raman scattering spectroscopy are powerful tools, enabling one to judge the microcrystal size, composition and other factors affecting lattice dynamics. Size effects in Raman spectra of microcrystals have been studied for BN [1], Si [2–5], Ge [3, 4], GaP [4], CdS [6] and other compounds.

Semiconductors of the $Sn_2P_2S_6$ family have become an object of extensive theoretical and experimental interest in view of phase transitions and polycritical phenomena observed under variations of temperature, pressure and mixed crystal composition [7–14]. $Sn_2P_2S_6$ crystals at ambient pressure undergo a second-order structural transition from the ferroelectric (Pn) to paraelectric ($P2_1/n$) phase at 337 K which was thoroughly studied by dielectric [15], Raman scattering [16–18], inelastic neutron scattering [10], ultrasonic [19], birefringence [20] and Mössbauer spectroscopy [21] measurements. In all cases the studies were carried out for good-quality bulk single crystals.

In $Sn_2P_2S_6$ ceramics with the grain size below 1 μm a decrease of the phase transition temperature by 12 K with respect to the bulk sample was observed by dielectric measurements [22]. It should be noted that nanocrystalline $Sn_2P_2S_6$ powders with average sizes down to 20 nm were obtained earlier by soft chemistry methods [23, 24], but no detailed Raman studies of such samples have been reported. Therefore, spectroscopic studies of both ceramic and powdered micro- and nanocrystalline $Sn_2P_2S_6$ samples seem to be helpful in order to find and explain the effects related to the decrease in size.

2. Experimental details

$Sn_2P_2S_6$ bulk single crystals were grown by chemical transport, the details of the growth technique being described in [25]. The microcrystalline powders of various grain sizes were obtained by ball milling the material in a stainless steel cylindrical vial with a hardened steel ball, similar to that described in [26]. A vibrating frame (type Fritsch Pulverisette 0) was used to keep in motion the vial and the ball. Prior to milling the vial was evacuated and then sealed. The 75 h milling process was interrupted after 5, 25 and 50 h periods and a small amount of powder was taken for investigation. The grain size reduction achieved during each milling step was followed by measuring the XRD spectra of powders with a horizontal Siemens diffractometer by using Cu $K_{\alpha 1}$ radiation.

For transmission electron microscopy (TEM) investigations the ball-milled powder was mixed with epoxy resin and a thin layer of this mixture was spread between two silicon wafers and embedded into an aluminium disc. After the epoxy had been cured the sample was ground and polished mechanically from both sides. The final thinning was performed with a low-angle ($<5^\circ$) Ar ion treatment. A JEOL 2000 FX-II transmission electron microscope equipped with an Oxford Link-Isis EDS system was used for the TEM measurements.

Two types of samples of $Sn_2P_2S_6$ ceramics were prepared from the powder fractions with average sizes $\sim$10 nm and $\sim$10 μm, which were pressed under 100–300 atm into compact 3–5 mm thick tablets 8 mm in diameter and then annealed at 720–820 K over 2–5 h in quartz ampoules with some amounts of additional phosphorus and sulfur (ratio 1:3) in order to provide the required counterpressure level.

For Raman scattering studies the powders were placed into a transparent optical container and measurements were performed in a backscattering geometry at room temperature on a LOMO DFS-24 double grating monochromator with a FEU-79 phototube and a photon counting system, the excitation being provided by a 25 mW He–Ne laser (632.8 nm). The instrumental width did not exceed 1 cm^{-1}. The measurements were performed at different acquisition times with different degrees of attenuation of the incident laser beam, in all cases the power density did not exceed 12 W cm^{-2}.

3. Results and discussion

Figure 1 illustrates a TEM image of one of the fractions of the $Sn_2P_2S_6$ microcrystalline powders obtained, from which the shape and average size of the grains can be evaluated. The grain size histograms, an example for one of the fractions being shown in figure 2, enabled us to estimate the average crystallite diameter and its mean-square deviation.

XRD analysis (figure 3) has confirmed that the $Sn_2P_2S_6$ lattice structure is preserved for the nanocrystalline samples, though the diffraction peaks become broader and less pronounced with the decrease in size. A doublet with Miller indices (110) and (112) was used for the halfwidth analysis. The width of the reflection profiles was determined by fitting Voigt

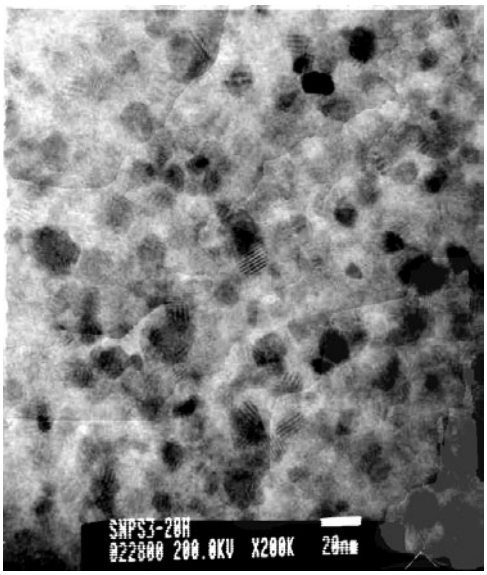

Figure 1. TEM image of $Sn_2P_2S_6$ powder after 25 h milling.

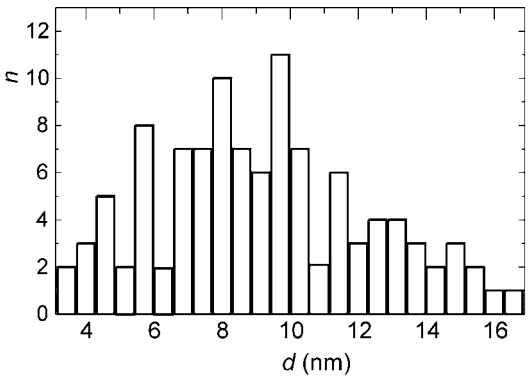

Figure 2. Distribution of the number of nanoparticles n over their average diameter d for $Sn_2P_2S_6$ powder after 75 h milling, based on TEM data.

functions to the XRD pattern and the grain size was calculated from the known Scherrer equation [27]:

$$d = \frac{\lambda}{\Delta(2\theta)\cos\theta_0} \tag{1}$$

where d is the average nanocrystal diameter, λ is the x-ray wavelength, $\Delta(2\theta)$ is the diffraction peak halfwidth and θ_0 is the diffraction angle. Thus obtained average grain size parameters (18, 13, 10 and 9 nm for the milling durations $t_m = 5, 25, 50$ and 75 h, respectively) have shown good agreement with those measured by TEM.

Room-temperature unpolarized Raman spectra of $Sn_2P_2S_6$ powders with different grain sizes are shown in figure 4 along with the bulk single-crystal spectrum. A detailed analysis of the $Sn_2P_2S_6$ Raman spectrum is reported in [18] (and references therein), so here we concentrate solely on the Raman features induced by the size decrease. Note that we did not observe

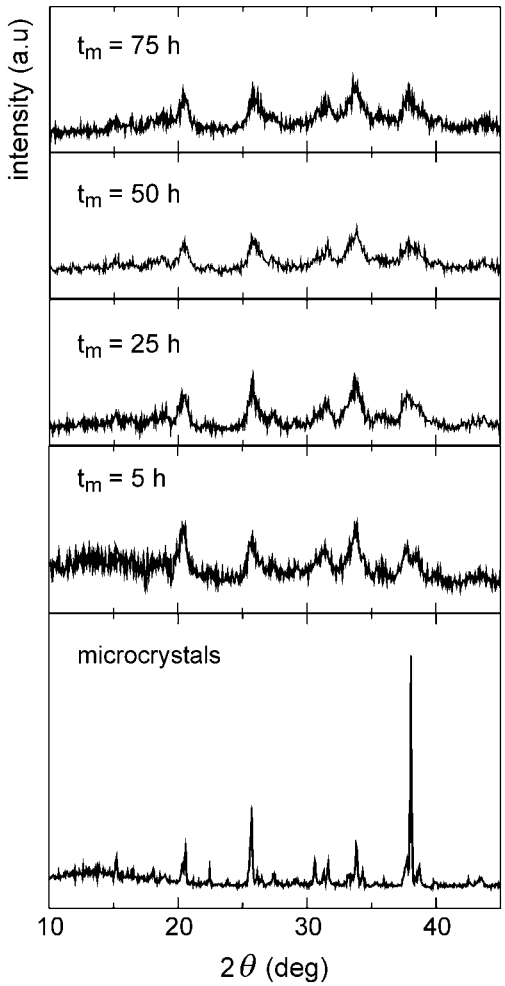

Figure 3. XRD patterns for microcrystalline and nanocrystalline $Sn_2P_2S_6$ powders.

changes in the spectra taken for the same samples at different acquisition times and incident power densities.

As seen from figure 4, the low-frequency part of the Raman spectrum cannot be resolved for the $Sn_2P_2S_6$ powder fractions with smaller grain sizes due to the considerable increase of Rayleigh scattering, masking the low-frequency Raman bands. However, most bands at the frequency above 100 cm^{-1} are clearly visible even for the samples with $d = 18$ nm ($t_m = 5$ h), and the most pronounced of them, centred near 381 cm^{-1}, is observed even for the finest powder fractions. This band corresponds to the stretching vibration of the P–P bond, joining the apices of two PS_3 pyramids in the anionic sublattice of the crystal. It is this particular band whose spectral position, width and shape variation under the powder grain size decrease was the main subject of our present Raman study.

That part of the experimentally observed $Sn_2P_2S_6$ Raman spectrum, corresponding to the P–P bond vibration band, is shown by triangles in figure 5 for powders with different grain sizes. It is clearly seen that the decrease of the crystallite average diameter is accompanied by a slight, but quite clearly noticeable, downward shift of the peak frequency (from 381 to

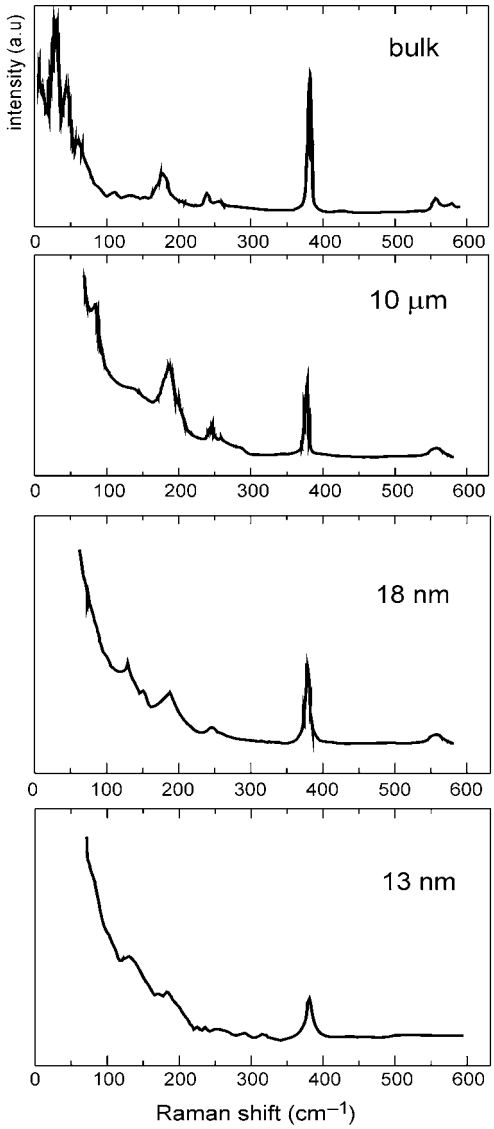

Figure 4. Raman spectra of bulk and nanocrystalline $Sn_2P_2S_6$.

379 cm^{-1}), an increase of its halfwidth (from 6.0 to 11.4 cm^{-1}) and some asymmetry, though the latter is not observed distinctly enough for all the samples and no general trend in the behaviour of the lineshape with the size parameter can be traced at a glance.

It should be noted that such behaviour of Raman band parameters on crystallite size is rather typical for semiconductor microcrystals whose Raman spectra have been thoroughly studied, e.g. for Si [2, 4, 5], GaP [4], $CdS_{1-x}Se_x$ [28–30]. Raman line broadening in polycrystalline and microcrystalline sample spectra can often be related to the selection rules violation resulting in the contribution of phonons with nearby frequencies active in other scattering geometries, but here it was not the case since, for both $Sn_2P_2S_6$ powders and bulk samples, unpolarized Raman spectra were measured.

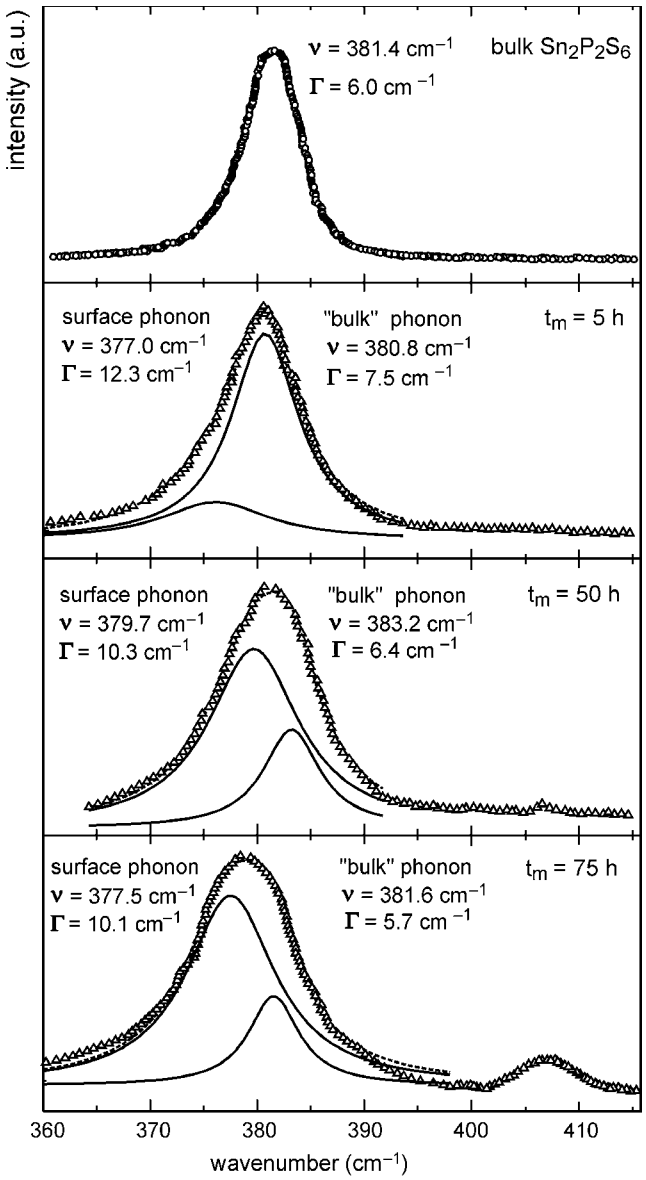

Figure 5. Part of the Raman spectrum, including the most intense band near 381 cm^{-1}, corresponding to the P–P bond vibration, for bulk and powdered $Sn_2P_2S_6$ and its simulation by two Lorentzian contours with the relevant parameters.

In Raman spectra of microcrystals two main factors are considered responsible for the peak frequency downward shift, the band broadening and a typically asymmetric shape with a more pronounced low-frequency wing, usually observed at the average diameter decrease—confinement-related selection rules relaxation due to the small crystallite size [5, 29–33] and surface phonon modes [28, 29, 34, 35].

When the crystallite size becomes finite, typically of the order of 10 nm, a phonon can no longer be described by a planar wave, but as a wavepacket whose spatial dimensions are

comparable to the crystallite size [5]. This introduces a spread or uncertainty in the wavevector q which increases with the grain size decrease because the wavepacket becomes more localized in space.

According to the phonon confinement model [5, 31], the first-order Raman spectrum $I(\omega)$ in a nanocrystalline semiconductor is given by

$$I(\omega) = \sum_j A_j \int \frac{\mathrm{d}^3 q |C(0, \vec{q})|^2}{[\omega - \omega_j(\vec{q})]^2 + (\Gamma_0/2)^2} \tag{2}$$

where j is the number of phonon bands, A_j is a coefficient, $\omega_j(\vec{q})$ is the phonon dispersion curve, Γ_0 is the linewidth (FWHM in the bulk crystal) and $C(0, \vec{q})$ is the Fourier coefficient of the phonon confinement function $W(\vec{r}, L)$, with L being the nanocrystal diameter and $\vec{r}$ the radius vector. The integration in equation (2) is performed over the entire Brillouin zone. The choice of appropriate confinement function, which depends on the nanocrystal geometry, is discussed in detail in [5, 31].

The average phonon dispersion for the jth phonon mode is usually taken as [29]

$$\omega_j(\vec{q}) = \omega_{j0} - \Delta\omega_j \sin^2(q/4). \tag{3}$$

There are no explicit experimental data regarding the dispersion of the phonon branch near 381 cm^{-1}, corresponding to P–P bond vibrations in $Sn_2P_2S_6$, across the Brillouin zone. Note that lattice dynamics calculations for crystals of such a type have shown very small dispersion for phonons above 200 cm^{-1} [36]. Therefore, it was reasonable to calculate, using equations (2) and (3), the confinement-related effects on the P–P bond vibration Raman lineshape for $Sn_2P_2S_6$ nanocrystals of different average sizes and different values of phonon dispersion $\Delta\omega$. Thus calculated dependences of the Raman band parameters are shown in figure 6. As can be seen from the figure, for the nanocrystal size, corresponding to the experimentally measured powders (9 nm), no confinement-related effects can be observed even for $\Delta\omega = 40$ cm^{-1}, which is far above the expected values. As follows from the calculations, even for considerably smaller nanocrystals the Raman peak downward shift and broadening due to the phonon confinement (see figure 6) should be much smaller than the values observed experimentally in our case. Thus, one may conclude that the confinement-related wavevector selection rules relaxation cannot be the main factor responsible for the observed size-dependent behaviour of the Raman band frequency, width and shape. Therefore another factor, namely scattering by surface phonon modes, should be invoked for an explanation.

Surface phonons in crystals are studied by the resonant Raman scattering technique when the exciting (or scattered) photon energy is close to the energy of an electronic transition in the crystal. In such a case due to a high absorption coefficient α the probing depth $1/2\alpha$ and, consequently, the scattering volume $V_\mathrm{s} = \pi d_\mathrm{b}^2/8\alpha$ (d_b being the laser beam diameter on the sample surface) is small enough to provide a considerable contribution of surface phonons to the observed spectra. In $Sn_2P_2S_6$ the exciting 632.8 nm light energy (1.96 eV) is considerably lower than the gap value (2.3 eV at 298 K [37, 38]), hence at such off-resonance conditions one could hardly observe surface phonons in bulk $Sn_2P_2S_6$. However, in the case of nanometric crystals the effective scattering volume can be related rather to the crystallite size parameter ($V_\mathrm{s} = \pi d_\mathrm{b}^2 d/4$) than to the probing depth since the light is scattered effectively only from the first layer of nanocrystals due to strong diffuse light scattering at the grain boundaries. For the nanocrystals of the first layer the surface phonon contribution is high enough to be taken into account. Moreover, if one even assumes the contribution of subsequent nanocrystal layers to be considered, for these crystallites the surface phonon contribution will be also of the same order due to the contribution of surfaces of each of these crystallites. Hence, contrary to the case of bulk materials, the contribution of surface phonons to the Raman spectrum

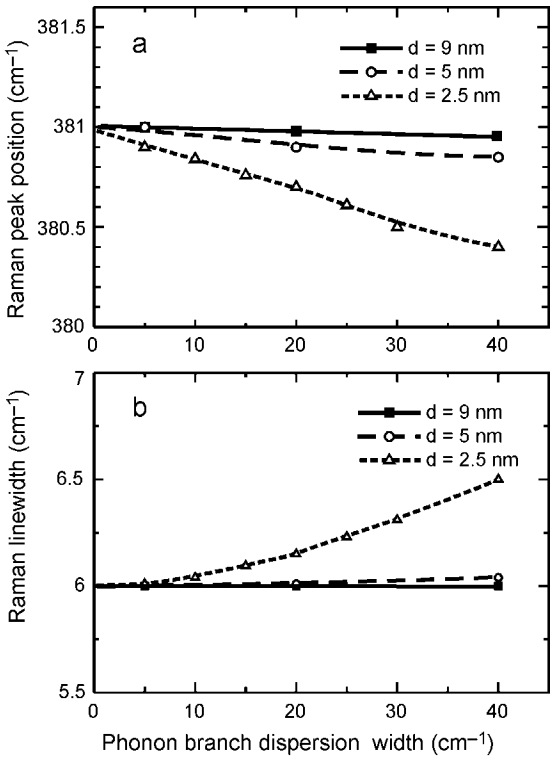

Figure 6. Calculated P–P vibration Raman peak position (a) and halfwidth (b) versus the phonon dispersion $\Delta\omega$ for different $Sn_2P_2S_6$ nanocrystal sizes.

of nanocrystalline powders should be taken into account independently of the exciting beam probing depth. Therefore, in spherical microcrystals of diameter d one might expect Raman observation of Fröhlich surface phonon modes, corresponding to

$$\varepsilon(\omega) = -\frac{(l+1)}{l}\varepsilon_{\mathrm{m}} \tag{4}$$

where $l = 1, 2, 3, \ldots$ and ε_{m} is the dielectric constant of the medium, surrounding the microcrystals [39].

The Raman scattering efficiency in a small spherical crystal is given by [39]

$$S = C|a\beta + b|^2\langle E^2\rangle\Delta(K, k) \tag{5}$$

where C is a constant, the quantities a and b give the magnitudes of the atomic displacement and electro-optical contributions to the scattering, $\langle E^2\rangle$ is the volume- and thermal-averaged squared field amplitude of a surface mode, and

$$\Delta(K, k) = \frac{1}{\pi}\frac{k'' + 1/R}{(K - k')^2 + (k'' + 1/R)^2} \tag{6}$$

where R is the radius of the sphere, K is the bulk phonon radial wavenumber, defined from the momentum conservation law, and k' and k'' are the real and imaginary parts of the complex radial wavenumber, introduced in order to include both bulk phonons (real values in the case of damping effects being neglected) and surface phonons (imaginary values) in the same

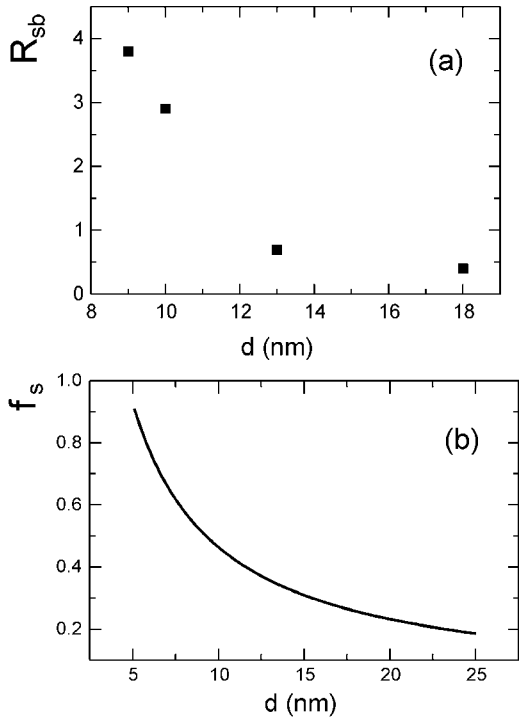

Figure 7. Dependences of experimental surface-to-bulk phonon integrated intensity ratio (a) and calculated fraction of unit cells adjacent to the surface (b) on the $Sn_2P_2S_6$ nanocrystal size parameter.

formulation. In the limiting case of a bulk crystal ($k'' = 0, 1/R \to 0)\Delta(K, k)$ tends to the delta function $\delta(K - k)$ [39]. For the Stokes and anti-Stokes Raman scattering

$$\langle E^2 \rangle = \begin{cases} \dfrac{8\pi}{V}[n(\omega)+1]\hbar\left(\dfrac{\mathrm{d}}{\mathrm{d}\omega}\varepsilon(\omega)\right)^{-1} & \text{(Stokes)} \\ \dfrac{8\pi}{V}[n(\omega)]\hbar\left(\dfrac{\mathrm{d}}{\mathrm{d}\omega}\varepsilon(\omega)\right)^{-1} & \text{(anti-Stokes)} \end{cases} \tag{7}$$

where V is the crystallite volume, $\varepsilon(\omega)$ is the dielectric constant and $n(\omega) = 1/[\exp(\hbar\omega/kT) - 1]$ [39].

In order to estimate the contribution of surface phonon modes to the experimentally measured spectra we have approximated the Raman peak, observed in the powder samples near 381 cm^{-1} by a superposition of two Lorentzian contours, the results being shown in figure 5. It is clearly seen that in all cases the observed band is well fitted by two peaks, the lower-frequency peak being broader (Γ = 10–13 cm^{-1}) than the higher-frequency one (6–8 cm^{-1}). The position of the peaks is almost the same for all samples. However, the surface-to-bulk phonon integrated intensity ratio R_{sb} strongly varies with the grain size, whose decrease results in the higher contribution of the lower-frequency band which makes the resulting band to shift down and broaden. Such behaviour enables us to attribute the broader lower-frequency band to the surface phonon in $Sn_2P_2S_6$. The peak asymmetry and downward shift with the grain size decrease results from the increase of the surface-to-bulk phonon intensity ratio (see figure 7(a)). It is quite evident since even simple estimations show: at the grain size of 20 nm the fraction f_s of about a quarter of the $Sn_2P_2S_6$ unit cells are located at the nanocrystal surface,

and at the crystallite diameter $d = 10$ nm half of the unit cells form the surface. The further decrease of d to 5 nm would make more than 90% of the crystallite unit cells need to be located at its surface (figure 7(b)), but we could not manage to obtain such small crystallites by milling, since the average grain size of the powder fractions with the milling duration above 50 h varies very slowly. Moreover, Raman spectroscopic studies of $Sn_2P_2S_6$ nanocrystals have enabled us to notice an additional feature which encumbers the further decrease of the powder grain size by this technique.

A careful look at the Raman spectrum of the finest powder fraction enables one to notice an additional band at 406 cm^{-1}, considerably weaker than the P–P bond vibration band (see figure 5). This band is observed quite clearly, which was confirmed by repeated measurements performed for another batch of $Sn_2P_2S_6$ powders after 75 h milling. The band can hardly be attributed to some confinement- or surface-related effects since there have been no phonons reported with slightly higher frequency in the bulk $Sn_2P_2S_6$ spectrum [18]. Since after the powders having been extracted from the container we could smell the presence of H_2S, we suspected the chemical reaction of partial oxidation of $Sn_2P_2S_6$ by water vapour in the air due to which part of the sulfur atoms at the nanocrystal surface were substituted by oxygen. It could happen when the powder was extracted from the vial before being put into a special container used for Raman measurements due to a highly extended surface of the nanometric powder. Since the surface-to-bulk ratio is much higher for the smaller nanocrystals, the discussed band at 406 cm^{-1} is clearly observed only for the finest powder fractions. There are no data available on the Raman spectra of $Sn_2P_2(S_{1-x}O_x)_6$ compounds. However, the measurements carried out for $Sn_2P_2(S_{1-x}Se_x)_6$ solid solutions [40] have shown the possibility of the variety of $(P_2S_{6-m}Se_m)^{4-}$ anions with partially ($m = 1, 2, \ldots, 5$) substituted chalcogen atoms to be formed. Moreover, the bands, corresponding to such groups, were clearly observed in the Raman spectra, particularly for the P–P bond vibration band, as distinct separate peaks with frequencies intermediate between those for $(P_2S_6)^{4-}$ and $(P_2Se_6)^{4-}$ anions [40]. The estimates of the anion reduced mass in our case show that the maximum at 406 cm^{-1} could correspond to the P–P bond vibration in $[P_2(S_4O_2)]^{4-}$ anions. If one assumes equal cross sections of Raman scattering for such oxygen-containing crystals and pure $Sn_2P_2S_6$, from the observed band intensity ratio the oxygen concentration in the finest powder fraction can be roughly estimated as $x = 0.1$. In such a case the probability of $[P_2(S_4O_2)]^{4-}$ anion formation is about 10% and the relevant Raman peak could be observed experimentally. One should also expect observation of a band at about 394 cm^{-1}, related to the $[P_2(S_5O)]^{4-}$ anion, for which the formation probability is estimated as 35% and, possibly, $(P_2S_{6-m}O_m)^{4-}$ anions with $m = 3, 4, 5$ whose probability of being realized is much smaller. However, no such bands are revealed experimentally, which indicates that in our case oxygen atoms preferably substitute sulfur in P_2S_6 anions in pairs. Since the $(P_2S_6)^{4-}$ anions structurally comprise two PS_3 pyramids, joined by a P–P bond, it can be assumed that only one sulfur atom in each pyramid is at the nanocrystal surface and therefore can be easily substituted by oxygen. However, we fail to give a reasonable enough explanation why this should preferably take place simultaneously for both pyramids of the same anion.

It should also be kept in mind that the phonon spectrum of the $Sn_2P_2S_6$ crystal is reported to contain another mode near 440 cm^{-1}, which is observed in Raman spectra as a very weak band only at low temperatures [18], as well as in Raman and infrared spectra of other crystals with $(P_2S_6)^{4-}$ anions [41]. Though generally one cannot *a priori* reject the possibility of the considerable 'softening' of such a band along with a sharp increase of its Raman cross section with the size reduction, however, we could find no reasonable enough arguments for such behaviour, and the assignment of the observed band at 406 cm^{-1} to the complexes with partial $S \rightarrow O$ substitution seems much more substantiated.

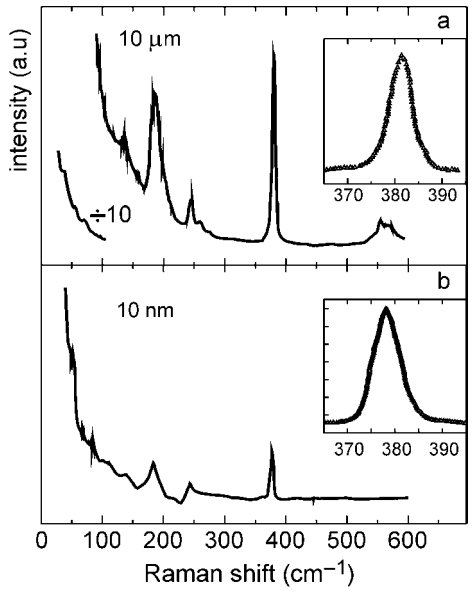

Figure 8. Raman spectra of 10 μm (a) and 10 nm (b) average grain size-based $Sn_2P_2S_6$ ceramics. The insets show the band near 381 cm^{-1} in more detail.

Raman spectra of $Sn_2P_2S_6$ ceramics are shown in figure 8. It is seen that, for both samples based on 10 μm and 10 nm grain sizes, the main Raman features of the $Sn_2P_2S_6$ crystal are preserved, though in the sample with smaller grains the band intensities are considerably smaller. It is worth noticing that, similarly to the case of $Sn_2P_2S_6$ powders, the decrease of the average grain size results in a slight downward shift of the frequency of the discussed P–P bond vibration maximum from 381 to 378 cm^{-1}, which is shown in the inset to figure 8. Meanwhile, contrary to the powders, in ceramics the band halfwidth is practically independent of the grain size ($\Gamma = 7$ and 6 cm^{-1}, respectively). It is hard to provide an unambiguous explanation for this difference in behaviour, though the surface effects should also play the predominant role in the case of ceramic samples with nanometric grains. Possibly, the reason for this may be related to the difference of the dielectric permeabilities, especially for the environment of the grains, in $Sn_2P_2S_6$ ceramics and powders. The most interesting feature in the Raman spectra of the nanometric-grain $Sn_2P_2S_6$ ceramics consists in the absence of the additional maximum slightly above the discussed P–P vibration band, which is observed in the powder samples with the same average grain size. This stands in favour of the above explanation of the nature of the discussed peak at 406 cm^{-1} as being related to oxygen-containing anions, since in the case of ceramics the samples were prepared in a phosphorus- and sulfur-rich atmosphere and the active surface area, subjected to oxidation, was much smaller than in the case of powders.

4. Conclusions

Nanometre-scale $Sn_2P_2S_6$ crystalline powders were obtained by milling, the average nanocrystal size ranging down to 9 nm, as estimated from XRD and TEM studies. X-ray and Raman scattering studies of the nanocrystalline powders and powder-based ceramic samples have shown the general resemblance of the spectra to those of similar bulk crystals, but with some additional features, specific for the Raman spectra of the finest powder fractions.

Namely, the observed slight downward shift and considerable broadening of the intense peak at 381 cm^{-1}, corresponding to the P–P bond vibration of the $(P_2S_6)^{4-}$ anions, with the average grain size decrease, is explained by the increasing role of the surface phonons due to the high surface-to-volume ratio in nanocrystals. The contribution of the confinement-related selection rules relaxation to the observed effect is discussed. An additional band at 406 cm^{-1}, revealed only for the finest powder fractions, is related to the partial substitution of sulfur in $(P_2S_6)^{4-}$ anions by oxygen at the nanocrystal surface.

References

[1] Nemanich R J, Solin S A and Martin R M 1979 *Phys. Rev.* B **20** 392
[2] Richter H, Wang Z P and Ley L 1981 *Solid State Commun.* **39** 625
[3] Gonzalez-Hernandez J, Azarbayajani G H, Tsu R and Pollak F H 1985 *Appl. Phys. Lett.* **47** 1350
[4] Hayashi S and Yamamoto K 1986 *Superlatt. Microstruct.* **2** 581
[5] Fauchet P M and Campbell I H 1988 *Crit. Rev. Solid State Mater. Sci.* **14** S79
[6] Vasilevskiy M I, Rolo A G, Gomes M J M, Vikhorova O V and Ricolleau C 2001 *J. Phys.: Condens. Matter* **13** 3491
[7] Gomonnai A V, Grabar A A, Vysochanskii Yu M, Belyayev A D, Machulin V F, Gurzan M I and Slivka V Yu 1981 *Fiz. Tverd. Tela* **23** 3602
Gomonnai A V, Grabar A A, Vysochanskii Yu M, Belyayev A D, Machulin V F, Gurzan M I and Slivka V Yu 1981 *Sov. Phys.—Solid. State* **23** 2093 (Engl. Transl.)
[8] Vysochanskii Yu M and Slivka V Yu 1992 *Usp. Fiz. Nauk* **162** 139
Vysochanskii Yu M and Slivka V Yu 1992 *Sov. Phys.—Usp.* **35** 123 (Engl. Transl.)
[9] Van Loodrecht P H M, Maior M M, Molnar S B, Vysochanskii Yu M, van Bentum P J M and van Kempen H 1993 *Phys. Rev.* B **48** 6014
[10] Eijt S W H, Currat R, Lorentzo J E, Saint-Grégoire P, Hennion B and Vysochanskii Yu M 1998 *Eur. J. Phys.* B **5** 169
[11] Eijt S W H, Currat R, Lorentzo J E, Saint-Grégoire P, Katano S, Janssen T, Hennion B and Vysochanskii Yu M 1998 *J. Phys.: Condens. Matter* **10** 4811
[12] Hlinka J, Janssen T and Dvořák V 1999 *J. Phys.: Condens. Matter* **11** 3209
[13] Smirnov M B, Hlinka J and Solov'ev A V 2000 *Phys. Rev.* B **61** 15051
[14] Berezovsky S V, Korda V Yu and Klepikov V F 2001 *Phys. Rev.* B **64** 064103
[15] Maior M M 1999 *Fiz. Tverd. Tela* **41** 1456
Maior M M 1999 *Sov. Phys.—Solid State* **41** 1333 (Engl. Transl.)
[16] Vysochanskii Yu M, Slivka V Yu, Voroshilov Yu V, Gurzan M I and Chepur D V 1979 *Fiz. Tverd. Tela* **21** 211
Vysochanskii Yu M, Slivka V Yu, Voroshilov Yu V, Gurzan M I and Chepur D V 1979 *Sov. Phys.—Solid State* **21** 123 (Engl. Transl.)
[17] Gomonnai A V, Vysochanskii Yu M, Grabar A A and Slivka V Yu 1981 *Fiz. Tverd. Tela* **23** 3623
Gomonnai A V, Vysochanskii Yu M, Grabar A A and Slivka V Yu 1981 *Sov. Phys.—Solid State* **23** 2105 (Engl. Transl.)
[18] Hlinka J, Gregora I and Vorliček V 2002 *Phys. Rev.* B **65** 064308
[19] Samulionis V, Banys J, Vysochanskii Yu and Grabar A 1999 *Phys. Status Solidi* b **215** 1151
[20] Vysochanskii Yu M, Mitrovcij V V, Grabar A A, Perechinskii S I, Motrja S F and Kroupa J 2000 *Ferroelectrics* **237** 193
[21] Baltrunas D, Grabar A A, Mazeika K and Vysochanskii Yu M 1999 *J. Phys.: Condens. Matter* **11** 2983
[22] Cho Y W, Choi S K and Vysochanskii Yu M 2001 *J. Mater. Res.* **16** 3317
[23] Bourdon X, Prouzet E and Cajipe V B 1997 *J. Solid State Chem.* **129** 157
[24] Bourdon X and Cajipe V B 1998 *J. Solid State Chem.* **141** 290
[25] Prits I P, Voroshilov Yu V and Potorii M V 1990 *Izv. Akad. Nauk SSSR Neorg. Mater.* **26** 2363
[26] Bakker H, Di L M and Lo Cascio D M R 1992 *Solid State Phenom.* **23/24** 253
[27] Guinier A 1956 *Théorie et Technique de la Radiocristallographie* (Paris: Dunod)
[28] Mlayah A, Brugman A M, Carles R, Renucci J B, Valakh M Ya and Pogorelov A V 1994 *Solid State Commun.* **90** 567
[29] Roy A and Sood A K 1996 *Phys. Rev.* B **53** 12127
[30] Ingale A and Rustagi K C 1998 *Phys. Rev.* B **58** 7197
[31] Campbell I H and Fauchet P M 1986 *Solid State Commun.* **58** 739

[32] Trallero-Giner C, Debernardi A, Cardona M, Menendez-Proupin E and Ekimov A I 1998 *Phys. Rev.* B **57** 4664
[33] Sirenko A A, Belitsky V I, Ruf T, Cardona M, Ekimov A I and Trallero-Giner C 1998 *Phys. Rev.* B **58** 2077
[34] Hayashi S and Ruppin R 1985 *J. Phys. C: Solid State Phys.* **18** 2583
[35] Hwang Y N, Park S H and Kim D 1999 *Phys. Rev.* B **59** 7285
[36] Bernasconi M, Marra G L, Benedek G, Miglio L, Jouanne M, Julien C, Scagliotti M S and Balkanski M 1985 *Phys. Rev.* B **38** 12089
[37] Ruediger A, Schirmer O, Odoulov S, Shumelyuk A and Grabar A 2001 *Opt. Mater.* **18** 123
[38] Studenyak I P, Mitrovcij V V, Kovacs Gy Sh, Mykajlo O A, Gurzan M I and Vysochanskii Yu M 2001 *Ferroelectrics* **254** 595
[39] Ruppin R 1975 *J. Phys. C: Solid State Phys.* **8** 1969
[40] Gomonnai A V, Vysochanskii Yu M, Gurzan M I and Slivka V Yu 1983 *Fiz. Tverd. Tela* **25** 1454
Gomonnai A V, Vysochanskii Yu M, Gurzan M I and Slivka V Yu 1983 *Sov. Phys.—Solid State* **25** 835 (Engl. Transl.)
[41] Joy P A and Vasudevan S 1993 *J. Phys. Chem. Solids* **54** 343